PRINT ISSN 1119-8362
Electronic ISSN 1119-8362

Full-text Available Online at
https://www.ajol.info/index.php/jasem
http://www.bioline.org.br/ja

J. Appl. Sci. Environ. Manage.
Vol. 25 (12) 2071-2083 December 2021

Equilibrium, Kinetic and Thermodynamic Studies of Dyes in Aqueous Solution onto Iron Nanocomposite Stabilized by *Irvingia gabonensis* Leaf Extract

***ADOWEI, P; EBONG, SE; OBUZOR, GU**

Department of Pure and Industrial Chemistry, Faculty of Science, University of Port Harcourt, Choba, Nigeria
**Corresponding Author Email: Pereware.adowei@uniport.edu.ng*

ABSTRACT: Elimination of dyes in contaminated water or wastewater has become a universal challenge because of their colouration, toxicity, mutagenicity and carcinogenicity when discharged into the recipient environment without treatment and several technologies have been developed to deal with this problem. This paper reports the potential of exploring the use and comparison of conventional iron zero-valent (nZVI) nanoparticle and *Irvingia gabonensis* stabilized iron nanocomposite (Ig-nZVI) for the elimination of methyl red (MR) and methyl orange (MO) dyes in aqueous solution under effect of different experimental conditions of adsorbent dosage, initial dye concentrations, pH, contact time and temperature. Data obtained show an increase in percent dye elimination as the amount of adsorbent increased. The optimal removal of MR and MO occurred in < 60 min of the start of each experimentation, obtained at a maximum pH of 5.1 at 98.5% and 80.6% for adsorbent dosage of 0.3g/50 mL and 20 mg/L initial dye concentration at temperature of 27ºC. The experimental data fitted the Lamgmuir isotherm with maximum adsorption capacity (q_{max}) of 166.7mg/g (Ig-nZVI) and 83.35 mg/g (nZVI) for MR while 128.21 mg/g (Ig-nZVI) and 40.02.5 mg/g (nZVI) were obtained for MO. Kinetics studies showed that the removal of MR and MO fitted the pseudo second-order model. The adsorption of MR and MO were endothermic and spontaneous with enthalpy values of 3.39kJ/mol (Ig-nZVI) and 776.26kJ/mol (nZVI) and standard Gibbs free energy values of -5.95kJ/mol (Ig-nZVI) and -12.00kJ/mol (nZVI). Thermodynamic studies ($\Delta G < 0$, $\Delta H < 0$, $\Delta S > 0$) implied a spontaneous and exothermic process in nature. The adsorption of MO was endothermic and spontaneous with enthalpy values of 31.70kJ/mol (Ig-nZVI) and 20.91kJ/mol (nZVI) and standard Gibbs free energy values of -5.92kJ/mol and -7.07kJ/mol for Ig-nZVI and nZVI respectively. Adsorbent produced from leaf extracts of African mango tree (*Irvingia gabonensis)* and stabilized by iron oxide could be an attractive option for elimination of dye from industrial effluents.

DOI: https://dx.doi.org/10.4314/jasem.v25i12.12

Dates: Received: 22 August 2021; Revised: 17 September 2021; Accepted: 06 October 2021

Keywords: African bush mango, nano-composite, Irvingia gabonensis, methyl red, Methyl orange

Dyes are principally used in the production of consumer products such as paints, textiles, printing inks, paper, and plastics (Kant, 2012). Rapid industrialization and urban development, have resulted in the generation of large quantities of aqueous effluents, many of which contain high levels of harmful pollutants such as organic dyes (Vijayaraghavan and Yun, 2008, Xu *et al.*, 2013). They pollute not only the environment but also pass through the entire food chain, leading to biomagnifications (Lin *et al.*, 2004; Gürses *et al.*, 2006; Li, 2010 and Gil *et al.*, 2011). Almost every industry uses dyes for their products. Dye industry effluents constitute one of the most challenging wastewaters to be treated not only for their high chemical oxygen demand (COD), biological oxygen demands (BOD) and reduction in dissolved oxygen (DO) of the water bodies but also for the colour they impart on these water bodies (Zawani *et al.*, 2009). Over the years, many physical, chemical and biological approaches have been employed for the evacuation of dyes from wastewater namely coagulation (Szygułaa *et al.*, 2009), precipitation (Zhu *et al.*, 2007), separation through membranes (Alventosa-deLara *et al.*, 2012), electrolysis (Wang, 2009), photolysis (Guo *et al.*, 2006), extraction (Abbassiana *et al.*, 2015), oxidation (Gomes *et al.*, 2012), biological treatments (Popli and Patel, 2015), and adsorption (Shaibu *et al.*, 2014) nevertheless with some setbacks (Wang *et al.*, 2010). Several popular low-cost adsorbents, including natural materials, biologically derived adsorbents, and waste materials from agricultural industries have also been used by some researchers (Namasivayam and Yamuna, 1992; Horsfall and Spiff (2005), Horsfall *et al* (2005), Adowei *et al* (2016), Ebong *et al.*, (2020), Tarawouu *et al* (2007); Namasivayam and Arasi 1997). The low-cost adsorbents are bedevilled with bulkiness in nature, slow adsorption kinetics, low capacity, disposal problems and re-generation, hence some authors have used activated carbon, hydrogen peroxide (H_2O_2), sodium hyperchlorite and other

**Corresponding Author Email: Pereware.adowei@uniport.edu.ng*

chemical agents for the textile industries effluents (Preethi *et al.,* 2006, Meshko *et al.,* 2001; Chen *et al.,* 2001, Purkait *et al.,* 2007; Chen *et al.,* 2011). Consequently, adsorbents such as nanocomposites (Adeyemo *et al.,* 2017) and zerovalent metals (Ponder *et al.,* 2000; Lin *et al.,* 2005; Xiong *et al.,* 2007; Wu *et al.,* 2009; Xu *et al.,* 2010; Wang *et al.,* 2010; Liu et al., 2010; Liu and Zhang, 2010) have become important for the removal of heavy metal ions, dyes and other pollutants from aqueous solution.

Recently, plant extracts are used to reduce metal ions to nanoparticles in a single-step green synthesis process (Saif *et al.,* 2016). This biogenic reduction of metal ion to base metal is quite fast, readily conducted at room temperature and pressure, and easily scaled up. Synthesis mediated by plant extracts is environmentally benevolent. The reducing agents involved include the various water soluble plant metabolites (e.g. alkaloids, phenolic compounds, terpenoids) and co-enzymes. Textile effluents containing dyes and other organic compounds require fast treatment due to their toxic health and environmental effects (Sayyad *et al.,* 2012; Siskova *et al.,* 2013). *Irvingia gabonensis* (Aubry-LeComte er O'Rorke) Bail (Irvingiaceae) commonly called wild mango or African bush mango or ogbono is a plant tree that occurs freely in Nigeria and produces an edible fresh mango-like fruit whose seed is used in the preparation viscous soup (Okogun, 2002; Abdulrahman *et al.,* 2004). *Irvingia gabonensis* has two fruiting seasons: from April to July and from September to October and produces huge amount of leaf droppings as waste. The fruit (Okogun, 2002), seed (Ngodi et al., 2005), stem bark (Mgbemena *et al.,* 2019) and root (Oben, 2011) has been investigated for various uses other than food, however, studies on the leaf is scanty. Due to the paucity of data on the leaf, this study explored the potential of employing the use and compare convention iron zerovalent (nZVI) nanoparticle and *Irvingia gabonensis* stabilized iron (Ig-nZVI) nanocomposites for elimination of methyl red (MR) and methyl orange (MO) in aqueous solution.

MATERIALS AND METHODS

Dye Used: The dyes used for this work are methyl red (MR) and methyl orange (MO) presented in figure 1a and b respectively. Other chemical reagents used were of analytical grade and acquired from representatives of Merck and Aldrich.

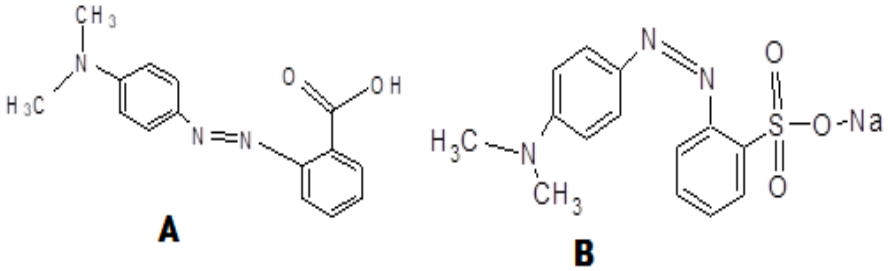

Fig 1: Structure of Methyl Red [A] and Methyl Orange [B]

Sample collection: Fresh leaves of African bush mango (*Irvingia gabonensis*) were collected from Delta Park University of Port Harcourt Rivers State, Nigeria. Taxonomical identification and authentication were carried out at the University of Port Harcourt Herbarium.

Sample Preparation and Synthesis: Fresh leaves were plucked from African bush mango (*Irvingia gabonensis*) tree and washed several times with tap water and finally two times with distilled water to remove dirt, bird droppings and other impurities. The washed leaves were sun dried for 5 hours to remove residual moisture. Dried leaves were grounded to powdery form and kept for further use as samples. The detailed procedure for the aqueous extraction, synthesis of zerovalent iron nanoparticles and preparation of African bush mango leaf extract stabilized by iron oxide has been published elsewhere (Ebong *et al.,* 2020).

Preparation of Calibration Curves for the Dyes (MR and MO): Preparation of Methyl Red (MR) and Methyl Orange (MO) Dye Solution: A stock solution of 1,000 mg L^{-1} was prepared by dissolving an appropriate 250 mg of MR and MO in separate 250 mL double-distilled water. Different concentrations of 5, 15, 25, 45, and 55 mg L^{-1} of dye were prepared from the stock solution. The sample concentrations were measured using a double beam UV-Vis spectrophotometer (U-2910, Hitachi, Tokyo, Japan) at room temperature (27^{o}C ± 2^{o}C) at their maximum absorption wavelengths.

*Batch Dye Elimination Studies: Effect of adsorbent dosage on adsorption***:** To 10 ml of dye (MR and MO) with 20 mg/L concentration in two identical 100ml

conical flask was added 0.02g 0.04g, 0.06g, 0.08g, 0.1g, 0.2g and 0.3g of Ig-nZVI and nZVI respectively and gently agitated for complete dispersion of the adsorbents with dye solutions and kept for 30mins. The reaction flask was again agitated after 30mins and filtered through Whatman filter paper number 1. The filtrates were stored in sterile plastic containers for determination of the final dye concentration using UV-Visible spectrometer.

Effect of initial concentration on adsorption: The influence of initial dye concentration on adsorption was studied at room temperature. The concentration of each dye solution was varied from: 5, 10, 15, 20 and 25 mg/l respectively. A measured mass of 0.3g of nZVI and Ig-nZVI was added to each initial concentration of dye solution. The mixture was agitated and equilibrated for 30 mins. The mixture was filtered and the filtrate collected into sterile plastic container for the determination of the final dye concentration using UV-Visible spectrometer.

Effect of pH on adsorption: The dye solutions with 20 mg/L concentration (MR and MO) were pre-adjusted to pH 3, 5, 7, 9 and 11 with the addition of either 0.1M HCl or 1M NaOH solutions. To 10 ml of dye solution at the different pH, in two identical 100ml conical flask was added 0.3g of Ig-nZVI and nZVI respectively and gently agitated for complete mixture of the adsorbents with the dye solutions and kept for 30 min, thereafter, the mixture was agitated again and filtered with Whatman filter paper number 1 and the filtrates were stored in sterile plastic containers for UV-visible analysis.

Effect of time on adsorption: To 10 ml of dye with 20 mg/L concentration solution in two identical 100ml conical flask, was added 0.3g of Ig-nZVI and nZVI respectively and gently agitated for complete mixture of the adsorbents with the dye solutions at room temperature (27^0C) and agitated again for 15 min, 30 min, 45 min, 60 min, and 75 min. At the end of each agitation time interval, the mixture was filtered using Whatman filter paper number 1 and the filtrate stored in sterile plastic containers for UV-visible spectroscopic analysis.

Effect of temperature on adsorption: To 10 ml of dye with 20 mg/L concentration in two identical 100ml conical flask was added 0.3g of Ig-nZVI and nZVI respectively and gently agitated for complete mixture of the adsorbents with the dye solutions and transferred to a thermostat water bath which was pre-set at 30^0C, 45^0C, 60^0C, 75^0C and 90^0C for 30 min. The reaction flask was removed from the water bath and agitated and filtered through Whatman filter paper number 1. The filtrates were stored in sterile plastic containers for UV-visible analysis.

*Analysis and Mass Balance Calculation***:** The concentration of dye (mg/L) in the solution was measured by direct UV-visible spectrophotometric method using Genesis 20 Thermo Scientific at optimum wavelength. All the experiments were duplicated, and only the mean values were reported. The amount of dye eliminated at equilibrium by the nZVI and Ig-nZVI, q_e (mg/g), were calculated by the mass balance relationship in equation 1:

$$q_e = \frac{C_O - C_e}{V} x\ W \qquad 1$$

Where C_O and C_e (mg/L) are the initial and equilibrium liquid-phase concentrations of dye, respectively, V is the volume of the solution (L), and W is the weight of nanocomposite used (g).

The percentage of dye eliminated from solution were calculated according to equation 2.

$$\%\ \text{Elimination} = \frac{C_O - C_e}{C_O} x100 \qquad 2$$

Where C_o (mg/L) is the initial dye concentration, C_e (mg/L) is the equilibrium concentration

Equilibrium Isotherm Studies: Equilibrium isotherm studies were obtained from the different concentrations of MR and MO measured at room temperature under the experimental procedures for the effect of concentration.
The linearized Langmuir and Freundlich equilibrium isotherm model equations were used to describe the experimental data.

Langmuir Equilibrium Isotherm Model Equation: The linear form of the Langmuir equation used is presented in equation 3:

$$\frac{C_e}{q_e} = \frac{1}{K_L q_m} + \frac{1}{Q_m} C_e \qquad 3$$

Where q_m is the maximum monolayer capacity of the adsorbent (mg/g), K_L is the adsorption equilibrium constant (L/mg).

A plot of $\frac{C_e}{q_e}$ versus C_e is expected to give a slope of $\frac{1}{q_m}$ and intercept of $\frac{1}{K_L q_m}$; which will be used to evaluate the maximum monolayer capacity (q_m) and the adsorption equilibrium constant (K_L).

Freundlich Equilibrium Isotherm Model Equation: The linear Freundlich isotherm equation employed for the evaluation of the experimental data is given in equation 4.

$$\log q_e = \log K_F + \frac{1}{n}\log C_e \qquad 4$$

Where K_F is the Freundlich adsorption or distribution coefficient and represents quantity of dye adsorbed onto the adsorbent for unit equilibrium concentration and $\frac{1}{n}$ is the adsorption intensity of dye onto the adsorbent or surface heterogenecity, becoming more heterogeneous as its value gets closer to zero

The applicability of the Freundlich adsorption isotherm was also analyzed using the same set of experimental data, by plotting $\log q_e$ vs $\log C_e$.

Kinetics Studies: Kinetic studies were obtained from the data for the effect of contact time of dye measured at room temperature. The kinetics of dye (MR and MO) onto nZVI and Ig-nZVI were analyzed using pseudo-first-order and pseudo-second order kinetic models.

Pseudo-first-order kinetic model equation: The linearized form of the Lagergren pseudo-first-order kinetic model equation used is presented in equation 5.

$$\log(q_e - q_t) = \log(q_q) - \frac{k_1}{2.303}t \qquad 5$$

Where q_e and q_t are the adsorption capacity at equilibrium and at time, t respectively (mg/g), k_1 is the rate constant of pseudo-first order adsorption (L/min).

A plot of log (q_e – q_t) versus t will be used to evaluate the Langergren constants.

Pseudo-second-order kinetic model equation: The linear form of the pseudo-second-order equation (6) used is presented as

$$\frac{1}{q_t} = \frac{1}{k_2 q_e^2} + \frac{1}{q_e}t \qquad 6$$

Where k_2 (g/mg min) is the second order rate constant of the adsorption process

The linear plots were made using $\frac{1}{q_t}$ versus t

Thermodynamic Studies: Thermodynamic parameters were computed from data obtained by measurement of temperature varied from 303 to 353 K. Thermodynamic parameters such as the thermodynamic equilibrium constant, K_e (Eqn. 7), change in standard Gibbs free energy, ΔG^o (Eqn. 8), change in standard enthalpy, ΔH^o (Eqn. 9), change in standard entropy, ΔS^o (Eqn. 10), and activation energy, E_a (Eqn. 11), were computed using the following equations:

$$K_e = \frac{q_e}{C_e} \qquad 7$$

$$\Delta G^O = -RT \ln K_e \qquad 8$$

$$G^O = H^O - T\Delta S^O \qquad 9$$

$$\ln K_e = \frac{\Delta S^O}{RT} - \frac{\Delta H^O}{RT} \qquad 10$$

$$\ln K_e = \ln A - \frac{E_a}{RT} \qquad 11$$

RESULTS AND DISCUSSION

The response of absorbance to different concentrations of MR and MO dyes were plotted (Fig 2a and b). The absorbance was measured at different concentrations of dye MR and MO. The linear portion of the calibration curve is fit with a line. The equation for MR is y = 0.0137x + 0.1564 with R^2 value of 0.9955 and that of MO is y = 0.0336x + 0.1056 with R^2 value of 0.9915. The equations were found to describe the relationship between absorbance and concentrations with correlation coefficients > 0.99.

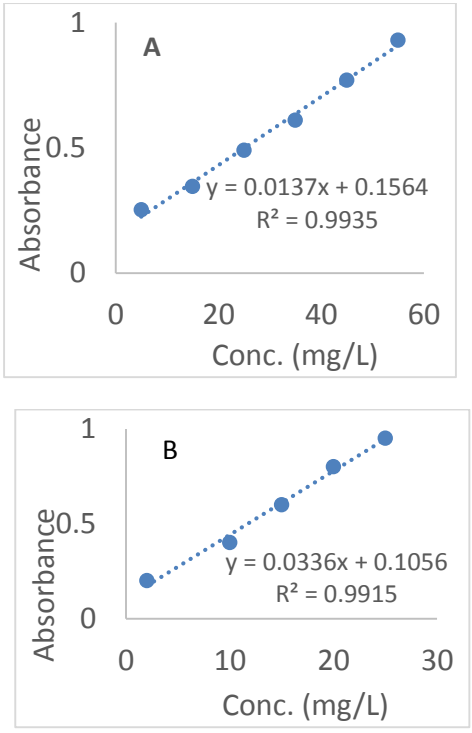

Fig 2. Calibration curve for methyl red (A) and methyl orange (B)

Effect of Adsorbent Dosage: According to Figure 3, the rate of elimination of both dyes increased with increase in the adsorbent (Ig-nZVI and nZVI) dose. At a dose of 0.02g, it was observed that 35.70% and 26.1% of MR was eliminated by Ig-nZVI and nZVI respectively while that of MO were 27.33% and 33.13% respectively. Subsequent doses of 0.04g, 0.06g, 0.08g and 0.1g correspondingly resulted in 48.10%, 71.40%, 88.61% and 94.17% elimination of MR by Ig-nZVI while the percentage elimination by nZVI occurred at 40.56%, 61.80%, 82.73% and 90.73% respectively. Results obtained for MO elimination showed that at doses of 0.04g, 0.06g, 0.08g and 0.1g, the percentage elimination increased to 57.17%, 78.10%, 82.2% and 89.00% for Ig-nZVI and 54.60%, 77.26%, 82.50% and 87.93% for nZVI respectively. The increase in adsorption with increase in adsorbent dose occurred as a result of increase in the surface area available for dye molecules to adsorb (Dada *et al*., 2015). The data showed that the percent elimination becomes constant for immediately after 0.1g adsorbent dose up to 0.3 g. Hence, the other experments were conducted using an adsorbent dose of 0.3 g.

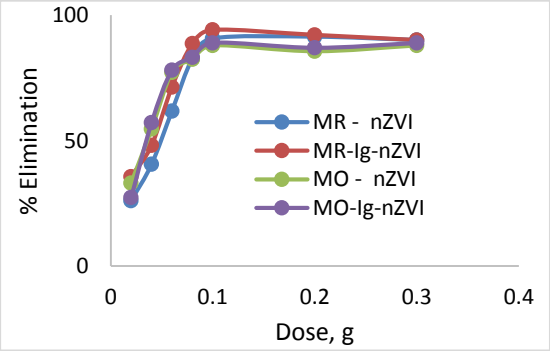

Fig 3: Effect of Adsorbent Dose on elimination of MR and MO with Ig-nZVI and nZVI

Effect of Initial Dye Concentration: The percentage elimination of MR and MO by both adsorbents decreased with an increase in initial dye concentration as shown in Figure 4. The elimination rates of MR by Ig-nZVI and nZVI were 98.5% and 80.6% respectively when the initial concentration of MR was 5mg/L and its elimination percentage reduced to 71.1% as the initial concentration was increased to10 mg/L. When the initial concentration was kept at 25mg/L, the elimination rate for both Ig-nZVI and nZVI dropped to 22.23% and 20.83%. In the case of MO, similar trend was observed; at initial concentration of 5mg/L, 80.63% and 74.10% of MO was eliminated by both Ig-nZVI and nZVI. On increasing the initial concentration to 10mg/L, percentage elimination dropped to 51.60% and 55.16% for Ig-nZVI and nZVI respectively. In addition, when the initial concentration was kept at 25mg/L, the elimination rate for both Ig-nZVI and nZVI dropped to 27.00% and 28.76%. The decrease in the elimination of both dyes in the aqueous media could be ascribed to a fixed amount (0.03g) of both adsorbents (Ig-nZVI and nZVI) with restricted adsorption sites which gets easily saturated, consequently, leading to a decrease in percentage elimination of both dyes corresponding to increasing initial concentration of both dyes. This agrees with the result reported by Siskova *et al.* (2013).

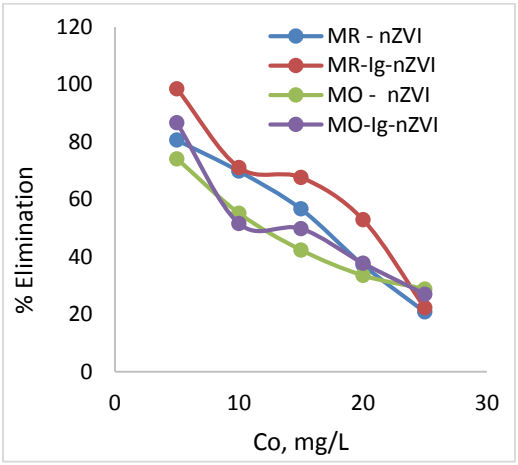

Fig 4: Effect of Initial Concentration on elimination of MR and MO with Ig-nZVI and nZVI

Effect of Time: At an initial contact time of 20 min, elimination efficiency of Ig-nZVI and nZVI for MR was fast with percentage elimination of 48.97% and 44.15%. A similar trend was observed for MO, with percentage elimination by Ig-nZVI and nZVI at 33.5% and 40.7% respectively. Percentage elimination of MR at contact time 30-45min for Ig-nZVI and nZVI increased from 61.40-72.93% and 51.37-67.43% respectively. For MO, an increase in percentage elimination was also observed at the same contact time range with values of 56.80-69.00% for Ig-nZVI and 42.50-52.53% for nZVI. After 60min, the elimination percentage of MR by Ig-nZVI and nZVI increased to 94.2% and 78.61% and that of MO by both adsorbents (Ig-nZVI and nZVI) also increased to 79.77% and 59.60%. However, on increasing the contact time to 75min, there was no significant elimination of both dyes; the percentage elimination obtained for MR was 96.43% and 80.75% for Ig-nZVI and nZVI respectively while that of MO was 81.5% and 61.70% for Ig-nZVI and nZVI respectively (Figure 5). This result could be attributed to the fact that at the initial stage, there were large numbers of unoccupied sites on the surface of the adsorbents (Ig-nZVI and nZVI) for adsorption. But as contact time increased, the

unoccupied sites became saturated, which lead to slow pore diffusion of the MR and MO molecules onto the adsorbents (Ig-nZVI and nZVI) and repulsion between the solid molecules and the bulk phases which is similar to the result of Karima *et al.* (2010).

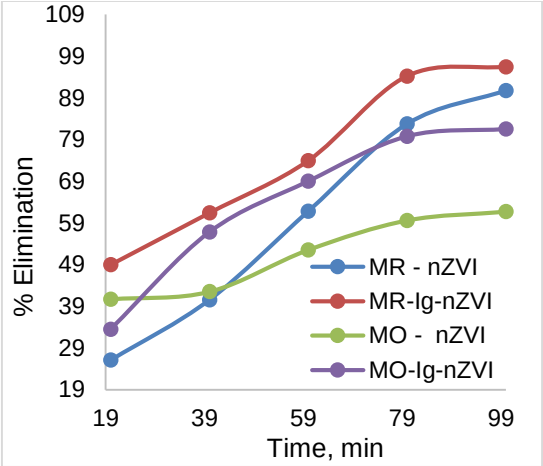

Fig 5: Effect of Contact Time on elimination of MR and MO with Ig-nZVI and nZVI

Effect of pH: During the adsorption process, functional groups, surface charges, degree of ionization and solubility of adsorbent are important factors which are influenced by pH of the aqueous solution. Results obtained for the elimination of dyes at various pH (Figure 6) increased from pH 2 to a maximum at about pH 5.1 and gradually decreased to pH 11. Percentage elimination of MR at pH 11, 9, 7, 5 and 3 were 37.3%, 41.5%, 50.3%, 80.33% and 54.6 respectively for Ig-nZVI and 54.7%, 56.4%, 57.3%, 64.4% and 59.4% respectively for nZVI. This is because at lower pH there were greater number of hydrogen ions present and thus, the degradation increased. The iron particles donate two electrons to the H^+ ions converting them into atoms which in turn attacks the dye particles present in the wastewater, breaking them down to amines and rendering them colorless (Chatterjee *et al.*, 2010). Likewise, the percentage elimination of MO from the aqueous medium increased with decreasing pH. At pH 5, the elimination efficiency increased from 93.83% to 95.63% and from 62.36% to 86.86% for Ig-nZVI and nZVI respectively. Whereas increasing the pH of dye solution to 7.0, 9.0 and 11 with the same amount of adsorbents (0.03g) at 27^0C and 10 min contact time a decrease in the elimination of both dyes was observed with values of 63.33%, 58.30% and 56.90% respectively for Ig-nZVI and 53.36%, 51.86% and 51.60% respectively for nZVI. The low adsorption capacity at alkaline pH may be attributed to a decrease in reducing power of nanoparticles due to covering of nanoparticle with corrosion products; there is also a change in the charge of ZVI surface from positive to negative at alkaline pH which causes a repulsion force between the dye and nanoparticles (Phenrat *et al.*, 2007).

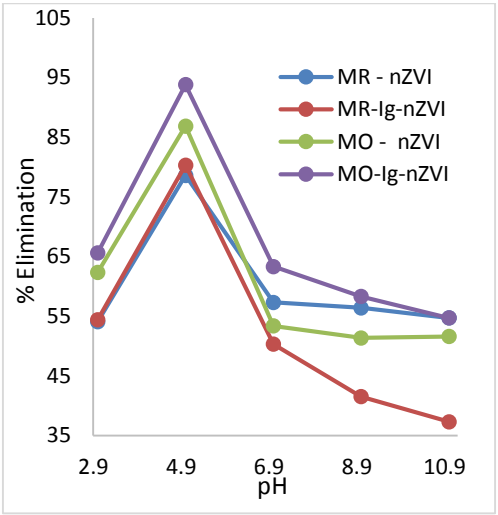

Fig 6: Effect of pH on elimination of MR and MO with Ig-nZVI and nZVI

Effect of Temperature: The elimination of MR and MO by nanoparticles (Ig-nZVI and nZVI) from aqueous media was controlled by temperature of the dye solutions. The result as shown in Figure 7 was evident that dye (MR and MO) elimination increased with increase in the temperature of the reaction. The elimination of MR by adsorbents (Ig-nZVI and nZVI) was found to increase from 26.43% to 38.73% and 32.53% to 42.50% respectively when the temperature was increased from 30^0C to 45^0C. On increasing the temperature further to 60^0C, 75^0C and 90^0C, Ig-nZVI gave an elimination percentage of 55.13%, 76.20% and 94.20% while results obtained for nZVI were 53.60%, 69.93% and 78.61% respectively. Results obtained for the elimination of MO by Ig-nZVI at temperatures 30^0C to 90^0C increased from 23.53% to 79.50% while results for nZVI at the same temperature range, increased from 20.47% to 74.97% respectively. The improvement in the elimination of MR and MO could be attributed to a reduction in the viscosity of the dye solution so that the mass transfer resistance to the adsorbate in the boundary layer decreases. In addition, increase the rate of dispersion of adsorbate molecules in the inner pores of adsorbent particles (Wang and Zhu, 2007; Dada *et al.*, 2015).

Equilibrium Isotherm Analysis: The relationship between the quantity of a substance adsorbed at constant temperature and its concentration in the aqueous solution is called the adsorption equilibrium isotherm. This isotherm is an excellent tool in

establishing the most appropriate correlations of the equilibrium data of each system which may aid the optimization and design of an appropriate adsorption system to eliminate the dye. To relate the experimental data, two mono-component isotherm models; the Langmuir and Freundlich isotherm models were employed.

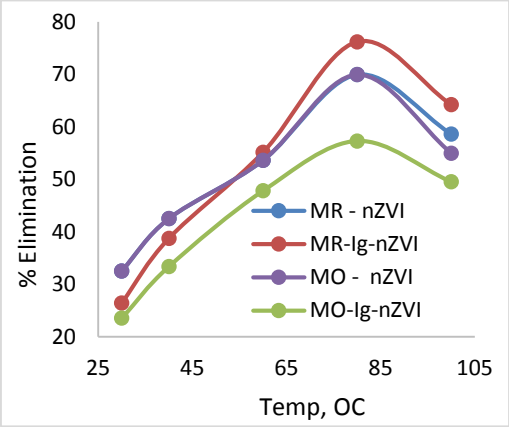

Fig 7: Effect of Temperature on elimination of MR with Ig-nZVI and nZVI.

Langmuir isotherm: The Langmuir adsorption isotherm model explains the variation of adsorption of adsorbates with concentration. It is based on the assumption that maximum adsorption occurs when a saturated monolayer of adsorbate molecules is present on the adsorbent surface, the energy of adsorption is constant, and there is no migration or interaction between the adsorbate molecules on the surface plane. The linear expression of the Langmuir isotherm model as expressed in equation 3 was used to obtain figure 8.

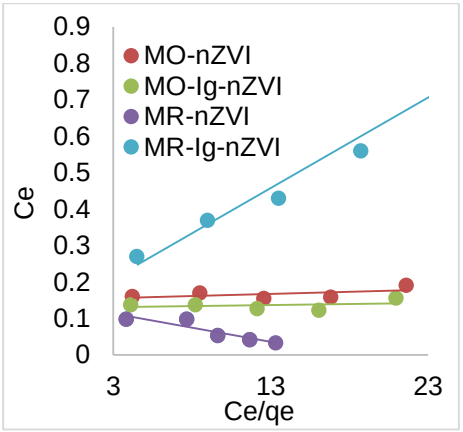

Fig 8: Langmiur isotherm of elimination of MR and MO by Ig-nZVI and nZVI

The Langmuir parameters obtained from Figures 8 are shown in Table 1. The elimination of MR by un-stabilized (nZVI) and *Irvingia gabonensis*-iron oxide-stabilized (Ig-nZVI) nanocomposite materials reveals that the Langmuir equilibrium constant, K_L (L/mg) related to energy of adsorption which quantitatively reflects the affinity between the adsorbent and adsorbate were computed as 0.079 and 0.046 respectively with R^2 values of 0.62 and 0.87. Also, elimination of MO by un-stabilized (nZVI) and *Irvingia gabonensis*-iron oxide-stabilized (Ig-nZVI) nanocomposite had K_L values of 0.057 L/mg and 0.185 L/mg respectively and an R^2 value of 0.845 and 0.9598 respectively. These values implied that the elimination process of MR and MO by un-stabilized (nZVI) and *Irvingia gabonensis*-iron oxide-stabilized (Ig-nZVI) nanocomposite was both partially linear and perhaps may be unfavourable and the data did not fit well to the Langmuir isotherm model. Hence, it can be inferred that the capacity of un-stabilized (nZVI) and *Irvingia gabonensis*-iron oxide-stabilized (Ig-nZVI) nanocomposites to eliminate both MR and MO in aqueous system is low based on the Langmuir isotherm model.

Freundlich isotherm: The Freundlich isotherm explains that the extent of adsorption varies directly with pressure. This empirical relationship describes the multilayer adsorption of heterogeneous systems and assumes that different sites have several adsorption energies involved (Horsfall and Spiff, 2005). The linear model of the Freundlich isotherm was used to logarithmically express as the experimental data (Figure 9). The Freundlich constants which gives an idea of the adsorption intensity and capacity, respectively were computed and are presented in Table 1.

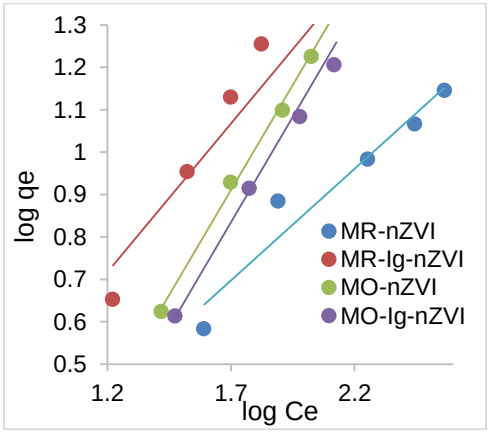

Fig 9: Freundlich isotherm of elimination of MR and MO by Ig-nZVI and nZVI

The results showed that, the degree of non-linearity between solution concentration and intensity of elimination depends on the heterogeneity which indicates the distribution of bonds and it is not

dependent on the concentrations of adsorbents. The degree of non-linearity between solution concentration and adsorption depends on n as follows: If n = 1, the adsorption is linear; if n<1, this implies that the adsorption process is chemical; if n >1, the adsorption is a favorable physical process (Kumar *et al.,* 2010; Shahbeig *et al.*, 2013; Youssef *et al.*, 2013). The investigation was carried out by the plot of log q_e vs log C_e (Figure 9). The values from the plot are presented in Appendix IV. K_f and 1/n was determined from the intercept and slope of the plot. The adsorption of MR onto Ig-nZVI and nZVI was favored by the Freundlich isotherm model with n values of 1.42 (Ig-nZVI) and 1.90 (nZVI) and R^2 values of 0.89 and 0.94 for Ig-nZVI and nZVI respectively. The adsorption of MO onto Ig-nZVI and nZVI was also favored by the Freundlich isotherm model with n values of 1.00 (Ig-nZVI) and 1.01 (nZVI) and R^2 values of 0.98 and 0.99 for Ig-nZVI and nZVI respectively. The higher values of n and R^2 for the adsorption of MR and MO onto Ig-nZVI and nZVI implied that the adsorption process was a favorable physical process. These values also indicate the affinity of MR and MO molecules for the nano-adsorbents (Ig-nZVI and nZVI). Hence it can be inferred that the adsorption of both MR and MO fitted well to the Freundlich isotherm model. A similar trend was observed by Shaibu *et al*. (2014).

Table 1. Elimination Equlibrium Isotherm parameters

Adsorbate-Adsorbents	Freundlich isotherms parameters			Langmuir Isotherm parameters		
	K_f (mg/g)(L/mg)$^{1/n}$	n	R^2	q_{max} (mg/g	K_L L/mg)	R^2
MO-nZVI	0.1397	1.006	0.9971	128.21	0.056849	0.845
MO-Ig-nZVI	0.1682	1.009	0.9792	40.02	0.184682	0.9598
MR-nZVI	0.6374	1.904	0.9413	83.35	0.07888	0.6231
MR-Ig-nZVI	0.7473	1.425	0.8927	166.7	0.046359	0.865

Table 2. Comparison of maximum elimination capacities with respect to MR and MO in the present study with those reported in the literature

Nano-composites	**q_{max}, mg/g**		**Reference**
	MR	**MO**	
CNT/Fe/CS composite	125	142.9	Jie *et al.*, 2015
Cork Activated composite	-	16.66	Haitham *et al*., 2019
PANI/glass composite	93	147	Fouad and Benlahbib, 2015
KOH-Activated polypyrrole-based	497.50	520.8	Alghamdi *et al*., 2019
Chitosan/kaoli/γ-Fe_2O_3	36.67	35.27	Jiang *et al*., 2011
Activated Pomelo peel waste	163.11	226.90	Zhang *et al.*, 2020
Potato peel powder	30.48	-	Enenebeaku et al., 2019
Phosphate Activated carbon	226.90	435.25	Equbal *et al*., 2018
Amidoxine composite	-	142	Nazia Rahman et al 2019
Water hyacinth biomass	23.833	-	Tarawou *et al.*, 2007
(nZVI	83.35	40.02	This Study
Ig-nZVI	166.7	128.21	This Study

*Comparison of Adsorption Capacities with Literature Data***:** The adsorption capacities of un-stabilized (nZVI) and *Irvingia gabonensis*-iron oxide-stabilized (Ig-nZVI) nanocomposite materials as well as of other adsorbents with respect to methyl red and methyl orange reported in the literature are presented in Table I and are compared with those obtained for this study.

The ultimate adsorption capacities compared were those calculated from a Langmuir-type isotherm at 30 degrees and at an optimum solution pH of 8.0. It is palpable that the adsorption capacities vary within a wide range for the different adsorbents, depending on the experimental conditions. However, of un-stabilized (nZVI) and *Irvingia gabonensis*-iron oxide-stabilized (Ig-nZVI) nanocomposite materials were found to have strong potential regarding the removal of methyl red and methyl orange.

Adsorption Kinetics: Kinetic models were employed in this study to determine the mechanism of adsorption of MR and MO onto Ig-nZVI and nZVI. In order to investigate the controlling mechanism of adsorption processes such as mass transfer and chemical reaction, the pseudo-first-order and pseudo-second-order kinetic models were applied to model the kinetics of dye adsorption onto nZVI and Ig-nZVI. The rate constant, k_{ad} and correlation coefficients for different dyes were computed from the linear plots of log ($q_e - q_t$) versus t (Fig 9) and are listed in Table 3. The correlation coefficients for the pseudo-first-order kinetic model are low. Moreover, a large difference of equilibrium adsorption capacity (q_e) between the experiment and calculation was observed, indicating a poor pseudo first-order fit to the experimental data. The result (Table 3C and Appendix V) showed that the data did not fit into the whole time of study range of pseudo first-order model which is in line with Sarat

and Valdya (2016) findings in the study of adsorption kinetics mechanism of blue 222 reactive dyes onto *R arrhizus*. This could be as a result of the external resistance or boundary layer giving rise to time lag (Ho & McKay, 1999).

In order to apply the pseudo-second-order equation as expressed in equation 7 (Ho and McKay 1999)

$$\frac{t}{q_t} = \frac{1}{h} + \frac{1}{q_e} t \qquad (7)$$

Showed that $h = kq_e^2$ (mg $g^{-1}min^{-1}$) can be regarded as the initial adsorption rate when $t \to 0$ and k is the pseudo-second-order rate constant of adsorption (g $mg^{-1}min^{-1}$). A plot of t/q_t versus t should give a straight line if pseudo-second-order kinetics are applicable and q_e, k and h can be determined from the slope and intercept of the plot, respectively. The plots of the linearized form of the pseudo-second-order reaction for the dues are shown in Fig. 10. The pseudo-first-order and pseudo-second-order rate constants determined from Figs. 9 and 10 are presented in Table 3, along with the corresponding correlation coefficients. The plot of t/q_t versus t for the pseudo-second-order model (Fig. 7) yields very good straight lines (correlation coefficient, R^2>0.99) as compared to the pseudo-first order plot. The pseudo-second-order rate constants were in the range of 0.0088 to 0.0963 g/mg-min. The theoretical values of q_e also agree very well with the experimental ones. Both facts suggest that the adsorption of the dyes by nZVI and Ig-nZVI follows the pseudo-second-order kinetic model, which relies on the assumption that chemisorption may be the rate-limiting step. In chemisorption, the metal ions stick to the adsorbent surface by forming a chemical (usually covalent) bond and tend to find sites that maximize their coordination number with the surface (Atkins, 1995). The pseudo-second-order kinetic analysis reveals that the value of the initial adsorption rates (h) increases with increase in the initial dye concentration. The lower the concentration of metal ions in the solution, the lower the probability of collisions between these species and, hence, the faster dye molecules can bond to the active sites on the surface of the adsorbent (Wong et al., 2003).

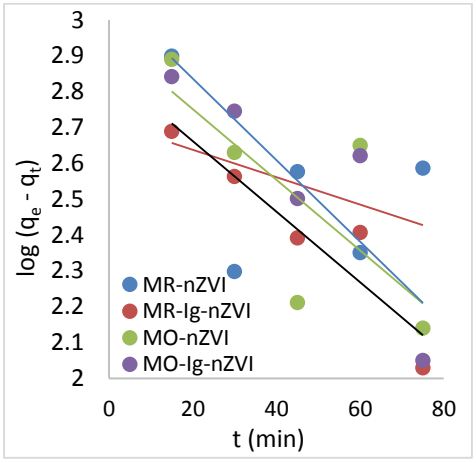

Fig 9: Pseudo-first-order kinetic plot for MR and MO elimination with nZVI and Ig-nZVI

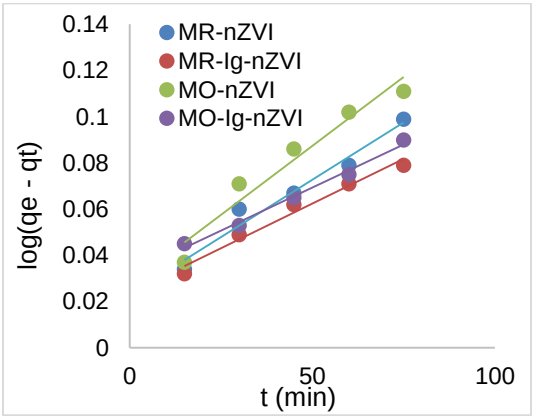

Fig 10: Pseudo-second-order kinetic plot for MR and MO elimination with nZVI and Ig-nZVI

Table 3 Kinetic parameters for elimination of MR and MO in aqueous solution by un-stabilized (nZVI) and *Irvingia gabonensis*-iron oxide-stabilized (Ig-nZVI) nanocomposite materials

	Pseudo first order		Pseudo second order	
Adsorbent	k_1(min^{-1})	R^2	k_2 (g/mg^{-1} min^{-1})	R^2
MO-nZVI	0.0228	0.5415	60168.47	0.942
MO-Ig-nZVI	0.026254	0.7663	89285.71	0.9899
MR-nZVI	0.008751	0.145	86580.09	0.9641
MR-Ig-nZVI	0.022569	0.8841	105042	0.9742

Table 4. Thermodynamic parameters () for the adsorption of MR and MO onto nZVI and nZVI

Adsorbents	ΔG kJ/mol	ΔH kJ/mol	ΔS kJ/mol	Ea kJ/mol	R>2
MO-nZVI	-6.951	-61.8797	-45.6181	-26.86917	0.953
MO-Ig-nZVI	-5.341	-84.02434	-70.5055	-36.48473	0.9485
MR-nZVI	-5.529	-85.60237	-73.2091	-37.16994	0.9838
MR-Ig-nZVI	-5.961	-88.74683	-75.1813	-38.53532	0.9858

Thermodynamics Studies: In order to evaluate the feasibility of the elimination process, the thermodynamic and activation energy parameters such as free energy, enthalpy and entropy changes were calculated using equations 7, 8, 9, 10 and 11. The data obtained from the effect of temperature on the adsorption of MR and MO onto Ig-nZVI and nZVI were tested with the adsorption thermodynamic equations. The thermodynamic parameters were determined from the Van't Hoff plot of 1/T versus log q_e/C_e. The standard enthalpy change ΔH^0 (kJ mol^{-1}) and standard entropy change ΔS^0 (J mol^{-1} K^{-1}) could be calculated from the slope and intercept of the plot with equations 10 (Boparai *et al.*, 2010; Ayanda *et al.*, 2013).

The elimination of MR and MO from aqueous media increased with an increase in temperature (Figures 4.11 and 4.12). This could be attributed to a reduction in the viscosity of the dye solution so that the mass transfer resistance to the adsorbate in the boundary layer decreases (Dada *et al.*, 2015). A positive value of enthalpy change (ΔH^0) 3.39 $kJmol^{-1}$ (Ig-nZVI) and 776.26 $kJmol^{-1}$ (nZVI) was obtained for the adsorption of MR onto Ig-nZVI and nZVI. A positive ΔH^0 showed that the adsorption of MR onto Ig-nZVI and nZVI were both endothermic (Figures 4.25 and 4.26). The standard entropy change (ΔS^0) values of 131.35 $JKmol^{-1}$ (Ig-nZVI) and 42.12 $JKmol^{-1}$ (nZVI) obtained for MR adsorption onto Ig-nZVI and nZVI indicated an increased degree of randomness at the solid–liquid interface during the adsorption of MR molecules onto Ig-nZVI and nZVI while the negative values of the standard Gibbs free energy (ΔG^0), 5.95$KJmol^{-1}$ and 12.0 $KJmol^{-1}$ indicated the feasibility and spontaneity of the adsorption process of MR onto Ig-nZVI and nZVI respectively.

Similarly, the positive ΔH^0 values of 31.707 $kJmol^{-1}$ and 20.908 $kJmol^{-1}$ for this study suggests that the adsorption of MO onto Ig-nZVI and nZVI respectively was endothermic (Figures 4.27 and 4.28). The standard entropy change (ΔS^0), 124.169 $JKmol^{-1}$(Ig-nZVI) and 92.327 $JKmol^{-1}$ (nZVI) indicated an increased degree of randomness at the solid–liquid interface during the adsorption of MO molecules by the adsorbates while the negative values of the standard Gibbs free energy (ΔG^0), 5.92 $KJmol^{-1}$(Ig-nZVI) and 7.07 $KJmol^{-1}$(nZVI) indicated the feasibility and spontaneity of the adsorption process of MO by Ig-nZVI and nZVI respectively. This result is similar to those reported by Hao *et al.* (2010) and Lisha *et al.* (2010).

Dye elimination was found to be associated with strong electrostatic forces (physisorption), the overall process being slightly endergonic ($\Delta G^0 > 0$). Our study shows that Ig-nZVI has a great potential of removing dyes from wastewater and other dye-polluted aquatic systems.

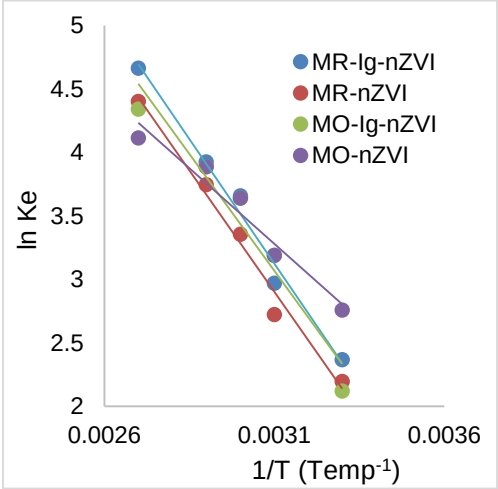

Fig 11: Thermodynamic plot for MR and MO elimination with nZVI and Ig-nZVI

Conclusion: Zerovalent iron nanoparticle and *Irvingia gabonensis* zerovalent iron nanoparticle were synthesized using sodium borohydride and *Irvingia gabonensis* aqueous leaves extract respectively. Both Ig-nZVI and nZVI eliminated methyl red and methyl orange from aqueous media but Ig-nZVI had better efficiency for removal of methyl red and methyl orange. This study has contributed to our knowledge on the utilization of nZVI and Ig-nZVI as an abundant, eco-friendly, low-cost alternative in the remediation of industrial effluents such as textile mill laden with organic dyes. Secondly, our knowledge on some of the functional groups present in Ig-nZVI, and nZVI has been shown. The various conditions of eliminating organic dyes from aqueous media using Ig-nZVI, and nZVI have established that nanocomposites are resourceful in the remediation of industrial effluents with organic dyes under these varying conditions. This has also added to our knowledge on how to employ these nano-adsorbents (Ig-nZVI, and nZVI) under varying conditions with respect to effluent treatment.

REFERENCES

Abbassian, K., Kargari, A; Kaghazchi, T. (2015). Phenol removal from aqueous solutions by a novel industrial solvent. *Chemical Engineering Communications*, *202*(3), 408-413.

Abdulaziz Ali Alghamdi., Abdel-Basit Al-Odayni *, Waseem Sharaf Saeed *, Mohammed S. Almutairi, Fahad A. Alharthi, Taieb Aouak and Abdullah Al-Kahtani Adsorption of Azo Dye Methyl Orange from Aqueous Solutions Using Alkali-Activated

Polypyrrole-Based Graphene Oxide (2019). *Molecules*, *24*(20), 3685

Abdulrahman, F; Inyang, I. S; Abbah, J; Binda, L; Amos, S and Gamaniel, K (2004). Effect of Aqueous Leaf Extract of Irvingia Gabonensis on Gastrointestinal Tract in Rodents. Indian Journal of Experimental Biology. 2(8):787-91.

Adeyemo, A. A., Adeoye, I. O., & Bello, O. S. (2017). Adsorption of dyes using different types of clay: a review. *Applied Water Science*, *7*(2), 543-568.

Adowei, A; Abia, A. A. (2016). Chemical Oxygen Demand (COD) Attenuation of Methyl Red in Water using Biocarbons obtained from Nipa Palm Leaves. J. Appl. Sci. Environ. Manage. 20 (4) 1163-1176

Bing Zhang, Yunhai Wu & Ligen Cha (2020) Removal of methyl orange dye using activated biochar derived from pomelo peel wastes: performance, isotherm, and kinetic studies, Journal of Dispersion Science and Technology, 41:1, 125-136, DOI: 10.1080/01932691.2018.1561298

Chen, Y. M., Tsao, T. M., & Wang, M. K. (2011). Removal of crystal violet and methylene blue from aqueous solution using soil nano-clays. In *International conference on environment science and engineering, IPCBEE* (Vol. 8, pp. 252-254).

Dada, A. O., Adekola, F. A., & Odebunmi, E. O. (2015). A novel zerovalent manganese for removal of copper ions: synthesis, characterization and adsorption studies. *Applied Water Science*, *7*(3), 1409-1427

Ebong, Sifon Emem, Adowei, Pereware, and Obuzor, Gloria Ukalina. (2020). Phytosynthesis and Characterization of Iron Nanocomposites by Irvingia Gabonensis (Ogbono) Aqueous and Ethanol Leaf Extracts. International Journal of Research 8(5), 256-265.

Enenebeaku, Conrad K; Nnaemeka J. Okorocha, Uchechi E. Enenebeaku, Ikechukwu C. Ukaga (2017). , "Adsorption and Equilibrium Studies on the Removal of Methyl Red from Aqueous Solution Using White Potato Peel Powder", International Letters of Chemistry, Physics and Astronomy. 72. 52-64

Equbal Ahmad Khan; Shahjahan Tabrez; Alam Khan (2018). Adsorption of methyl red on activated carbon derived from custard apple (*Annona squamosa*) fruit shell: Equilibrium isotherm and kinetic studies. Journal of Molecular Liquids. 249 (1) 1195-1211

Fouad Krika & Omar el Farouk Benlahbib (2015) Removal of methyl orange from aqueous solution via adsorption on cork as a natural and low-coast adsorbent: equilibrium, kinetic and thermodynamic study of removal process, Desalination and Water Treatment, 53:13, 3711-3723,

Gil, A., Assis, F. C. C., Albeniz, S., & Korili, S. A. (2011). Removal of dyes from wastewaters by adsorption on pillared clays. *Chemical Engineering Journal*, *168*(3), 1032-1040.

Gomes, A. C., Fernandes, L. R., & Simões, R. M. (2012). Oxidation rates of two textile dyes by ozone: effect of pH and competitive kinetics. *Chemical engineering journal*, *189*, 175-181.

Guo, Z., Ma, R., & Li, G. (2006). Degradation of phenol by nanomaterial TiO_2 in wastewater. *Chemical engineering journal*, *119*(1), 55-59.

Gürses, A., Doğar, Ç, Yalçın, M., Açıkyıldız, M., Bayrak, R., & Karaca, S. (2006). The adsorption kinetics of the cationic dye, methylene blue, onto clay. *Journal of Hazardous Materials*, *131*(1), 217-228.

Haitham, K; S. Razak, M. A. Nawi (2019). Kinetics and isotherm studies of methyl orange adsorption by a highly recyclable immobilized polyaniline on a glass plate. Arabian Journal of Chemistry. Volume 12, Issue 7, November 2019, Pages 1595-1606

Horsfall, M. Jnr and Spiff, A. I. (2005). Distribution of Trace Metals and Fulvic Acids in Sediments of the New Calabar River, Port Harcourt, Nigeria. *Asian Journal of Water, Environment & Pollution; pg. 75 – 79.*

Horsfall, M. Jnr.; and Spiff, A. I. (2005). Sorption of Lead, Cadmium, and Zinc on Sulfur-Containing Chemically Modified Wastes of Fluted Pumpkin (*Telfaria occidentalis)* HOOK f.). *Chem. & Biodiversity; Vol. 2; pp 373 – 385.*

Jiang, R; Zhu, H. and Yongqian Fu (*2011)*, "Equilibrium and Kinetic studies on adsorption of methyl orange from aqueous solution on chitosan/kaolin/γ-Fe2O3 nanocomposite," *2011 International Conference on Remote Sensing, Environment and Transportation Engineering*, Nanjing, 2011, pp. 7565-7568, doi: 10.1109/RSETE.2011.5966122.

Jie Ma; Yuan Zhuang; and Fei Yu (2015). Equilibrium, kinetic and thermodynamic adsorption studies of organic pollutants from aqueous solution onto CNT/C@Fe/chitosan composites. New Journal of Chemistry. 12: 9035 - 9986

Kant, R (2012). Textile dyeing industry and environmental hazard. Natural Science. 4. (1): 22-26.

Karima, B., Mossab, B. L., & A-Hassen, M. E. N. I. A. I. (2010). Removal of methylene blue from aqueous solutions using an acid activated Algerian bentonite: equilibrium and kinetic studies. In *International renewable energy congress* (pp. 1-8).

Li, S. (2010). Removal of crystal violet from aqueous solution by sorption into semi-interpenetrated networks hydrogels constituted of poly (acrylic acid-acrylamide-methacrylate) and amylose. *Bioresource technology*, *101*(7), 2197-2202.

Lin, C. J., Lo, S. L., & Liou, Y. H. (2005). Degradation of aqueous carbon tetrachloride by nanoscale zerovalent copper on a cation resin. *Chemosphere*, *59*(9), 1299-1307.

Lin, S. H., Juang, R. S., & Wang, Y. H. (2004). Adsorption of acid dye from water onto pristine and acid-activated clays in fixed beds. *J. Hazardous Mat. 113*(1), 195-200.

Liu, T., Zhao, L., Sun, D., & Tan, X. (2010). Entrapment of nanoscale zero-valent iron in chitosan beads for hexavalent chromium removal from wastewater. *J. Hazardous Mat. 184*(1), 724-730.

Liu, Z., & Zhang, F. S. (2010). Nano-zerovalent iron contained porous carbons developed from waste biomass for the adsorption and dechlorination of PCBs. *Bioresource technology*, *101*(7), 2562-2564.

Mandal, D., Bolander, M. E., Mukhopadhyay, D., Sarkar, G., & Mukherjee, P. (2006). The use of microorganisms for the formation of metal nanoparticles and their application. *Appl. Microbiol. Bbiotechn. 69*(5), 485-492.

Meshko, V., Markovska, L., Mincheva, M., & Rodrigues, A. E. (2001). Adsorption of basic dyes on granular acivated carbon and natural zeolite. *Water research*, *35*(14), 3357-3366.

Mgbemena, Nkoli Marynnn; Ilechukwu, Ifenna; Okwunodolu, Felicia Uchechukwu; Chukwurah, Joe-Vera, Ogugua and Lucky, Isioma Blessing (2019). Chemical composition, proximate and phytochemical analysis of *Irvingia gabonensis* and *Irvingia wombolu* peels, seed coat, leaves and seeds. Ovidius University Annals of Chemistry. 30 (1): 65 - 69, 2019

Mittal, A. K., Chisti, Y., & Banerjee, U. C. (2013). Synthesis of metallic nanoparticles using plant extracts. *Biotechnology advances*, *31*(2), 346-356.

Namasivayam, C., & Arasi, D. J. S. E. (1997). Removal of congo red from wastewater by adsorption onto waste red mud. *Chemosphere*, *34*(2), 401-417.

Namasivayam, C., & Yamuna, R. T. (1992). Removal of congo red from aqueous solutions by biogas waste slurry. *Journal of Chemical Technology and Biotechnology*, *53*(2), 153-157.

Nazia Rahman, Nirmal Chandra Dafader, Abdur Rahim Miah & S. Shahnaz (2019) Efficient removal of methyl orange from aqueous solution using amidoxime adsorbent, International Journal of Environmental Studies, 76:4, 594-60

Ngondi, J. L., Oben, J. E., & Minka, S. R. (2005). The effect of Irvingia gabonensis seeds on body weight and blood lipids of obese subjects in Cameroon. *Lipids in health and Disease*, *4*(1), 12 20

Oben, J. E. (2011). Seed Extract of the West African Bush Mango (Irvingia Gabonensis) and its Use in Health. Nuts and Seeds in Health and Disease Prevention pp. 1187-1189 https://doi.org/10.1016/B978-0-12-375688-6.10140-9

Okogun, Joseph I. (2002). Drug discovery through ethnobotany in Nigeria: some results. Advances in Phytomedicine. 1. 145-154

Phenrat, T., Saleh, N., Sirk, K., Tilton, R. D., & Lowry, G. V. (2007). Aggregation and sedimentation of aqueous nanoscale zerovalent iron dispersions. *Environ. Sci. Techn. 41*(1), 284-290.

Ponder, S. M., Darab, J. G., & Mallouk, T. E. (2000). Remediation of Cr (VI) and Pb (II) aqueous solutions using supported, nanoscale zero-valent iron. *Environ. Sci. Tech. 34*(12), 2564-2569.

Popli, S., & Patel, U. D. (2015). Destruction of azo dyes by anaerobic–aerobic sequential biological treatment: a review. *Inter. J. Environ. Sci. Tech. 12*(1), 405-420.

Preethi, S., Sivasamy, A., Sivanesan, S., Ramamurthi, V., & Swaminathan, G. (2006). Removal of safranin basic dye from aqueous solutions by adsorption onto corncob activated carbon. *Ind. Chem. Res. 45*(22), 7627-7632.

Purkait, M. K., Maiti, A., DasGupta, S., & De, S. (2007). Removal of congo red using activated carbon and its regeneration. *J. Hazardous Mat. 145*(1), 287-295.

Saif, S., Tahir, A., & Chen, Y. (2016). Green synthesis of iron nanoparticles and their environmental

applications and implications. *Nanomaterials*, *6*(11), 209.

Sayyad, A. S., Balakrishnan, K., Ci, L., Kabbani, A. T., Vajtai, R., & Ajayan, P. M. (2012). Synthesis of iron nanoparticles from hemoglobin and myoglobin. *Nanotechnology*, *23*(5), 055602.

Shaibu, S. E., Adekola, F. A., Adegoke, H. I., & Ayanda, O. S. (2014). A comparative study of the adsorption of methylene blue onto synthesized nanoscale zero-valent iron-bamboo and manganese-bamboo composites. *Materials*, *7*(6), 4493-4507.

Siskova, K. M., Straska, J., Krizek, M., Tucek, J., Machala, L., & Zboril, R. (2013). Formation of zero-valent iron nanoparticles mediated by amino acids. *Procedia Environ. Sci. 18*, 809-817.

Szyguła, A., Guibal, E., Palacín, M. A., Ruiz, M., & Sastre, A. M. (2009). Removal of an anionic dye (Acid Blue 92) by coagulation–flocculation using chitosan. *J. Environ. Manage. 90* (10), 2979-2986.

Tarawou, T. and Horsfall, M. Jnr (2007). Adsorption of Methylene Blue Dye on Pure and Carbonized Water Weeds. *Bioremediation J 11.2,1 – 8.*

Tarawou, T; Horsfall, M. Jnr and Vicente, J L (2007). Adsorption of Methyl Red using Water hyacinth (*Eichornia crassipes*) Biomass. *Chemistry & Biodiversity* 4 22 36 – 2245.

Vijayaraghavan, K. & Yun, Y.S. (2008). Bacterial biosorbents and biosorption.*Biotechnol. Adv.26*, 266–291.

Virkutyte, J., & Varma, R. S. (2013). Green synthesis of nanomaterials: environmental aspects. In *Sustainable nanotechnology and the environment: advances and achievements* (pp. 11-39). American Chemical Society.

Wang, L. (2009). Aqueous organic dye discoloration induced by contact glow discharge electrolysis. *J. Hazardous Mat. 171*(1), 577-581.

Wang, Q., Qian, H., Yang, Y., Zhang, Z., Naman, C., & Xu, X. (2010). Reduction of hexavalent chromium by carboxymethyl cellulose-stabilized zero-valent iron nanoparticles. *J. Contaminant hydrology*, *114*(1), 35-42.

Wang, S., & Zhu, Z. H. (2007). Effects of acidic treatment of activated carbons on dye adsorption. *Dyes and Pigments*, *75*(2), 306-314.

Wu, S. J., Liou, T. H., & Mi, F. L. (2009). Synthesis of zero-valent copper-chitosan nanocomposites and their application for treatment of hexavalent chromium. *Bioresource Tech. 100*(19), 4348-4353.

Xiong, Z., Zhao, D., & Pan, G. (2007). Rapid and complete destruction of perchlorate in water and ion-exchange brine using stabilized zero-valent iron nanoparticles. *Water Res. 41*(15), 3497-3505.

Xu, F. L., Jorgensen, S. E., Shimizu, Y., & Silow, E. (2013). Persistent organic pollutants in fresh water ecosystems. *Sci. World J. 2013*.

Xu, X., Wang, Q., Choi, H. C., & Kim, Y. H. (2010). Encapsulation of iron nanoparticles with PVP nanofibrous membranes to maintain their catalytic activity. *J. Membrane Sci. 348*(1), 231-237.

Zawani, Z., Chuah, A. L., & Choong, T. S. Y. (2009). Equilibrium, kinetics and thermodynamic studies: adsorption of Remazol Black 5 on the palm kernel shell activated carbon. *Europ. J Sci. Res. 37*(1), 67-76.

Zhu, M. X., Lee, L., Wang, H. H., & Wang, Z. (2007). Removal of an anionic dye by adsorption/precipitation processes using alkaline white mud. *J. Hazardous Mat. 149*(3), 735-741.